3D imaging of ZnO NP distribution and ROS accumulation in MCF-7 cells and quantification of retention dynamics using laser scanning confocal microscopy

Aishee Dey¹, Gare Suman², Sarpras Swain², Proma Bhattacharya¹, Vaibhav Dhyani², Lopamudra Giri², and Sudarsan Neogi¹

December 12, 2020

Abstract

Abstract Generally, investigations on nanomedicine involve conventional imaging techniques for obtaining static images on nanoparticle internalization at a single time point where various phases can be overlooked. In contrast, 3D live-cell imaging can be used for obtaining cellular retention of drugs at various phases, and cells can be followed for days. This article demonstrates the application of time-lapse microscopy in the investigation of Poly-L-lysine coated ZnO nanoparticle dynamics. In this work, a laser scanning confocal microscope has been employed to quantify the dynamics of internalization particles and reactive oxygen species generation (ROS) using volumetric imaging. Firstly, we show that simultaneous spatial mapping of nanoparticle uptake in MCF-7 cells and ROS in a single cell can be used to identify the interdependence between the accumulation of particles and ROS generation. Secondly, monitoring of ROS formation and cytotoxicity using the same imaging platform offers an advantage over monitoring these parameters using various instruments. Finally, the ability of the fluorescent particles in inducing a significant reduction in cell viability suggests its potential to be used as a therapeutic agent. The proposed framework opens up a new avenue of research for investigating mechanistic aspects of ZnO particle adsorption in vitro through long term imaging. Keywords: Fluorescent ZnO particle, Time-lapse microscopy, 3D Live-cell imaging, laser scanning confocal microscope, Reactive oxygen species

3D imaging of ZnO NP distribution and ROS accumulation in MCF-7 cells and quantification of retention dynamics using laser scanning confocal microscopy

Aishee Dey^a, Suman Gare^b, Sarpras Swain^b, Proma Bhattacharya^a, Vaibhav Dhyani^b, Lopamudra Giri*^b, Sudarsan Neogi*^a

Lopamudra Giri

Department of Chemical Engineering

Indian Institute of Technology, Hyderabad

NH 65, Sangareddy, Telangana 502285, India

Ph No: +91-40-12345678 Fax No: +91-40-23016032,

¹Indian Institute of Technology Kharagpur

²Indian Institute of Technology Hyderabad

^aDepartment of Chemical Engineering, Indian Institute of Technology, Kharagpur, India-721302

^bDepartment of Chemical Engineering, Indian Institute of Technology, Hyderabad, India- 502285

Email: giril@che.iith.ac.in

* corresponding author

Abstract

Generally, investigations on nanomedicine involve conventional imaging techniques for obtaining static images on nanoparticle internalization at a single time point where various phases can be overlooked. In contrast, 3D live-cell imaging can be used for obtaining cellular retention of drugs at various phases, and cells can be followed for days. This article demonstrates the application of time-lapse microscopy in the investigation of Poly-L-lysine coated ZnO nanoparticle dynamics. In this work, a laser scanning confocal microscope has been employed to quantify the dynamics of internalization particles and reactive oxygen species generation (ROS) using volumetric imaging. Firstly, we show that simultaneous spatial mapping of nanoparticle uptake in MCF-7 cells and ROS in a single cell can be used to identify the interdependence between the accumulation of particles and ROS generation. Secondly, monitoring of ROS formation and cytotoxicity using the same imaging platform offers an advantage over monitoring these parameters using various instruments. Finally, the ability of the fluorescent particles in inducing a significant reduction in cell viability suggests its potential to be used as a therapeutic agent. The proposed framework opens up a new avenue of research for investigating mechanistic aspects of ZnO particle adsorption in vitro through long term imaging.

Keywords: Fluorescent ZnO particle, Time-lapse microscopy, 3D Live-cell imaging, laser scanning confocal microscope, Reactive oxygen species

Introduction

Breast cancer treatment includes various modalities like surgery, radiation therapy as well as drug therapy for the prevention of metastasis. Since these drugs have prominent cytotoxic effects on both cancerous and healthy cells, there is a significant effort in developing biocompatible nanoformulations that can be tailored to their intended applications as therapeutics (). Determination of bioavailability and toxicity of such nanoparticles (NPs) require the use of imaging approaches, ideally with 3D capabilities. Monitoring cell-NP interaction for tumor cells using high-resolution imaging may provide insights on the attachment of particles on the cell surface (Song et al., 2015; Wang, Lee, Kim, & Zhu, 2017; Xia et al., 2008; Kiefer et al., 2020). In order to quantify the amount of internalized particles, it is crucial to perform imaging of various z-sections and perform 3D reconstruction of fluorescent intensity using confocal microscopy. Recent advancement in 3D visualization of nanoparticles distribution in living cells and tissue involves volumetric imaging using laser scanning confocal microscopy (LSCM) (Dias, Werner, Ward, Fleury, & Baulin, 2019; Ramos-Gomes, Ferreira, Kraupner, Alves, & Andrea Markus, 2020).

Drugs encapsulated in liposomes and polymeric NPs were found to be under clinical trials for the treatment of breast cancer (). In contrast, metal-based nanosystems, including gold, magnetic NPs, are still in the preclinical stage therapeutics (). Although there are some investigations focusing on the preliminary evaluation of ZnO toxicity in MCF-7 cell line (Supplementary Table S1) (Sadhukhan et al., 2019; ; Sureshkumar, Jothimani, Sridhar, Santhosh, & Venkatachalapathy, 2017;), there are limited data generation focusing on retention dynamics of ZnO particles. One of the major challenges in generating preclinical data is to develop particles that could be used for 3D imaging in live cells for a prolonged period of time (Dias et al., 2019; Ramos-Gomes et al., 2020). Here we demonstrate the synthesis of a fluorescent ZnO NP with Poly-L-lysine (PLL) coating that can be imaged for a longer period using confocal microscopy and also facilitates preferential uptake in tumor cells. These NPs were specifically tailored to exhibit the fluorescence at 488 nm through the addition of an optimal amount of Tween-80, and imaging of particle internalization was performed up to 72 hours. To quantify the amount of internalized particles in cells, we perform imaging of various z-sections and 3D reconstruction of fluorescent intensity.

Zinc oxide NPs have been shown to be effective in killing cancer cells for a wide range of cancer cell lines and reducing tumor size (Hussein & Ministry of health –clinical pathology center, 2017; Tanino et al., 2020; Sivakumar, Lee, Kim, & Shim, 2018). Additionally, it has been used for various biomedical applications

due to its long proven biocompatibility (; . Some form of Zn-based particles has been used as antiviral compounds that are known to be effective against the virus (Ghaffari et al., 2019; Tavakoli et al., 2018; Abdul, Muhammad, Ullah, Asmat, & Abdul, 2020; Faten & Ibrahim, 2018). Although, multiple investigations show that intact and modified versions of ZnO can be used to suppress MCF-7 cell growth and proliferation in vitro(; ; Boroumand Moghaddam et al., 2017; ; ; Wahab et al., 2014), in-depth preclinical studies are required focusing on quantification. Generally, fluorescent microscopy has been used for studying the internalization of ZnO particles (Hong et al., 2011; Sadhukhan et al., 2019; Ma et al., 2015). However, 3D imaging and quantification of particle internalization dynamics for a longer period are not possible if the particle is not optimized for imaging with confocal microscopy. There are few attempts to formulate fluorescent ZnO so that the particle can be monitored through 2D imaging using confocal microscopy (Sureshkumar et al., 2017; Gupta et al., 2015; Wang et al., 2017; Xia et al., 2008) . A summary of fluorescent ZnO particles that can be used for suppressing breast cancer cell lines are presented in Supplementary Table S1 .

Recent advancement in the synthesis of multifunctional particles focuses on intrinsic and extrinsic fluorescent zinc oxide particles for targeting MCF-7 cells. One of the studies focuses on the synthesis of fluorescent ZnO nanowires using vapor deposition in a similar size range, and the internalization in MCF-7 was detected within an hour at a concentration of 30 µg/mL (Hong et al., 2011; Ma et al., 2015). Ma et al. (2015) synthesized fluorescent ZnO quantum dots that shows that the particles are effective in regulating cell proliferation. Sureshkumar et al. (2017) synthesized polyquaternium capped zinc oxide nanodisc and used as an anticancer agent against MCF-7 cells. The synthesized NPs were found to be more stable than the commercial dyes, but the internalization dynamics was shown only for a short duration of 6 hours. One of the recent studies on particle internalization was performed using fluorescence microscopy using 2D imaging during the early phase of 1.5 hours (Sadhukhan et al., 2019). While most of these studies focus on the synthesis of the particle and viability studies, they do not elucidate the retention dynamics of ZnO particles and reactive oxygen species (ROS) generation. One of the studies shows that zinc oxide particles tagged with FITC were able to induce ROS generation in MCF-7 cells. Cell viability study was performed in the range of 8-500 μg/mL, whereas the cellular uptake of ZnO was studied at 100 μg/mL (Gupta et al., 2015) (Supplementary Table S1). Although this study reveals that ZnO can be used as a potential candidate for inhibiting MCF-7 cell proliferation and ROS generation, FITC is more prone to photobleaching, which may hamper the long-term imaging study.

Although ZnO particles can be imaged using 405 nm, excitation at higher wavelength is crucial to avoid cell apoptosis due to prolonged exposure to nearly UV light range during 3-day imaging. In order to address this, we demonstrate the synthesis of ZnO particles, where the concentration of Tween-80 was optimized to maintain the required level of fluorescence to be obtained through excitation at 488 nm. The rationale behind coating of the particles with Poly-L-lysine (PLL) is to enhance the biocompatibility and resisting photobleaching enabling long-term monitoring of the fluorescence during live imaging. It has been shown previously that PLL can be used for increasing the biocompatibility (Babic et al., 2008; Marsich et al., 2012),

The existing cytotoxicity studies were performed in the range of 24-48 hours. However, most of the ZnO internalization studies in MCF-7 cells were performed for approximately six hours using 2D imaging that provides information on the surface attachment of the particles. For example, the cellular uptake of FITC tagged ZnO with a size range from 100 - 400 nm was studied for up to 3 hours (Gupta et al., 2015). Since the time required for particle uptake can be shortened using smaller size particles, fluorescent ZnO nanorods in the range of 10 nm were shown to be internalized within 90 minutes in MCF-7 cells (Ma et al., 2015). Similarly, internalization of ZnO tagged with fluorescent drugs in the range of 30-40 nm was studied in MCF-7 cells between 3 and 6 hours (Sureshkumar et al., 2017; Sadhukhan et al., 2019). To the best of our knowledge, there is no investigation focusing on optimization of a nanostructure that can be used for 3D live-cell imaging of MCF-7 cells for a prolonged period. In this article, we demonstrate z-stack imaging of ZnO uptake, ROS formation, and cell fate imaging for up to 72 hours using fluorescent ZnO.

In order to show that the PLL coated ZnO particle can be used for simultaneous monitoring of internalization, we present the imaging assay using laser scanning confocal microscopy (LSCM) attached with a CO₂ incubator. One of the major novelties of the proposed assay includes the generation of data based on 3D imaging of ZnO internalization and ROS formation. In order to depict the spatiotemporal distribution of the particle and the correlation between NP internalization and ROS production, we have shown the spatial intensity mapping after merging the z-stacks. While most of the existing studies on ZnO NP internalization has been performed at 1 - 6 hour range (Sadhukhan et al., 2019; Hong et al., 2011; Ma et al., 2015; Sureshkumar et al., 2017; Gupta et al., 2015), the current work focuses on assessing the particle distribution using 3D imaging for three days. This study demonstrates that PLL coated particles in the range of 30 nm remain fluorescent over a longer period of time than fluorescent. Moreover, we show that the particle internalization, ROS formation, and viability can be monitored in the same imaging platform to assess the therapeutic potential in MCF-7 cell lines. Our results demonstrate that 3D imaging using LSCM represents a promising and powerful approach for preclinical investigations, which offers advantages of performing high-resolution imaging in living cells over other methods of volumetric imaging in fixed cells (Chen et al., 2013; Gimenez et al., 2016)

2. Materials and Methods

2.1 Materials: Zinc nitrate hexahydrate, Tween-80, ammonium carbonate, sodium hydroxide, and ethanol of analytical grade were purchased from Loba Chemie Private Limited. Dulbecco's Modified Eagle medium (DMEM), fetal bovine serum, MitoSOX Red, Propidium Iodide, Calcein, Poly-L-lysine solution, and PBS buffer were procured from Sigma- Aldrich.

2.2 Synthesis of NPs

- 2.2.1 Synthesis of ZnO_T NPs: The NPs were prepared using 0.25 M zinc nitrate hexahydrate solution, to which Tween 80 was added. The mixture was stirred at 50°C and homogenized, followed by dropwise addition of 0.25 M ammonium carbonate solution. The pH of the reaction mixture was maintained at 10, and the solution was further mixed at 80°C. Particles were washed with ethanol and dried in a hot air oven at 50°C overnight (Khan et al., 2010).
- **2.2.2 Synthesis of ZnO_T_PLL NPs**: The ZnO_T NPs were incubated in 0.1% (w/v) of PLL and kept overnight at 37 for 8 hours. The particles were centrifuged and dried at 37.
- 2.3 Controlling fluorescence of NPs using Tween-80: In order to have higher fluorescent signal of the particle, the concentration of Tween-80 in the precursor solution was varied as 8%, 12%, 14%, and 20% (v/v). The dry particles having fluorescence were characterized using LSCM (Leica SP8 microscope, Germany). The XYZY scanning was performed to obtain the excitation and emission wavelength range for the ZnO_T_PLL particle with the 40X oil emulsion objective. The coated and uncoated particles were further immersed and ultrasonicated at 20kHz in DMEM for quantification of the fluorescence of the particles with time.
- 2.4 Characterization of the NPs: The surface morphology and microstructural evaluation of the synthesized ZnO_T and ZnO_T_PLL NPs were investigated by Field emission scanning electron microscopy (FESEM) ((JEOL JSM-7610F FESEM with JEOL JEC-3000FC coater) and Transmission electron microscope (TEM) (JEM-2100 HRTEM, JEOL, JAPAN with an accelerating voltage of 20keV). The elemental analysis was done with Energy Dispersive X-Ray Spectroscopy (EDX). Dynamic light scattering (DLS) (Malvern Zeta-sizer ZS90 Nano-series (UK)) was used to analyse the hydrodynamic diameter of the particles whereas Zeta Potential (Malvern Zeta-sizer ZS90 Nano-series (UK)) was used to find the surface charge. Fourier Transform Infrared Spectroscopy (FTIR) (PERKIN ELMER SPECTRUM FTIR) techniques helped in confirming the functional groups present and the successful coating of PLL.
- 2.5 Cell culture: MCF-7/L929 cells were cultured in DMEM supplemented with 10% dialyzed fetal bovine serum and antibiotics. The cells were seeded (cell density of 2.047x10⁴ cells/mL) in 29 mm glass-bottom dishes and maintained with 5% CO₂in a humidified incubator at 37 °C.
- 2.6 Cellular Internalization Study: ZnO NPs at a concentration of 40µg/mL were added to the cells and incubated. Images were captured using LSCM at 0h, 12h, 24h, 36h, 48h, and 72 h after adding NPs

using 40X oil emulsion objective with 488 nm excitation. In order to quantify the extent of internalization of NP, the 3D images were merged in one plane, and the summation of fluorescence intensity was quantified using Leica LAS X software (Venkateswarlu et al., 2020). In order to have unbiased sampling, the LAX software was used for random sampling of three regions for various time points (**Supplementary Figure S1**). Various kinetic models were fit into the internalization data, and the pseudo 1st order kinetic model was found to be the best model with highest R² value of 0.988. Pseudo 1st order kinetic model used is:

$$Log(I_f-I_t) = log(I_f)-kt \dots (1)$$

Where I_f is the fluorescence intensity at 72 hours, I_t is the fluorescence intensity at time t, and I_f is considered to be the maximum intensity and hence maximum possible internalization.

- 2.7 ROS Generation Study: MitoSOX, a mitochondrial superoxide indicator, was used for measuring reactive oxygen species which exhibits red fluorescence upon binding with generated superoxide. MCF-7 cells were incubated with 40µg/mL of ZnO_T_PLL NPs for varying time periods. 1ml of 5µM MitoSOX red was added to cells and incubated for 10 minutes. The cells were thoroughly washed with a warm buffer at 37, and imaging was performed at an excitation and emission wavelength of 510 nm, and 574-751 nm respectively.
- 2.8 Cell Viability Study: The percentage of dead cells induced by ZnO_T_PLL NPs was measured using propidium iodide (PI) (excitation and emission at 493 and 636 nm respectively), a red fluorescent nuclear stain that enters only cells with disrupted plasma membranes. The unaffected status of the live cells was verified by detecting the green fluorescent signal due to calcein formation in them. Calcein-AM, a nonfluorescent dye known to permeate to the cytoplasm easily, is converted to a green fluorescent calcein (excitation and emission at 495 and 515 nm respectively) after acetoxymethyl ester hydrolysis by intracellular esterases in live cells. The cells were incubated with 40µg/mL NPs for varying time periods. calcein-AM, and PI were added in a 1:4 ratio to the cells and incubated for 20 minutes. The cells were then washed with a warm buffer at 37 and was used for further imaging. Live cells (Green) and dead cells (red) were counted for calculating the percentage of viability using the formula given below.

 $\% Viability = (N/N_{Total})*100.$ Where N represents the number of live cells, and N_{Total} represents the total number of cells.

- 2.9 3D reconstruction of MCF-7 cells: Multiple z-stacks corresponding to different focal planes were scanned in order to construct 3D images of cells internalized with fluorescent zinc oxide NPs. The fluorescence intensity of cells was measured by taking a total of 38 z stacks, which provided us the sample thickness varying between 30-40 μ m. We performed the quantification of percentage internalization of NPs at different time points using the merged images obtained from 2D images of individual planes (Supplementary Figure S2). A summary of the imaging parameters used for imaging using LSCM is shown in Supplementary Table S2 .
- **2.10 Statistical Analysis:** Data were presented as mean \pm standard deviation (SD). ANOVA and paired t-test was performed in statistical evaluation by MS-Excel. A p- value below 0.0001 was considered to be statistically significant.

3. Results and Discussions

3.1 Synthesis of fluorescent ZnO NPs and optimization of fluorescence: A facile chemical method was employed to synthesize the fluorescent zinc oxide NPs as represented in **Figure 1**. A LSCM was employed to perform a detailed study on the optical properties of the synthesized fluorescent particles. First, we performed XYZY scanning in confocal microscopy, which suggested that these particles can be imaged using excitation at 405 and 488 nm with an emission wavelength in the range of 415-460 and 504-668 nm, respectively (**Supplementary Figure S3**). Since lower wavelength is not suitable for live imaging for longer period of time, 488 nm was used as the excitation wavelength for all the nanoparticle retention studies.

Figure 2(a) and (b) show that fluorescence intensity increases with Tween-80 concentration. Since we aim

to retain fluorescence till 72hour, 20% (v/v) Tween-80, was selected for further investigations. Additionally, to retain the fluorescence in DMEM media and to obtain a slower release, the ZnO_T particles were coated by PLL. The dispersion of the ZnO_T and ZnO_T_PLL NPs in DMEM media along the course of 72 hours has been shown in **Figure 3(a)** and(b). The time course of fluorescence intensities, as shown in **Figure 3(c)**, demonstrated a significantly more retained fluorescence (p<0.0001) of the ZnO_T_PLL NPs over ZnO_T NPs. The result clearly shows that PLL encapsulation is able to retain the particle fluorescence level for a longer period of time. In order to justify the ability of the NPs to be stored and transported, the fluorescence of dry ZnO_T_PLL NPs was monitored over a period of one year, as shown in **Supplementary Figure S4**. The particles were found to retain their fluorescence over three months, showing a potential for transportation and storage.

3.2 Characterization of NPs: FESEM images (Figure 4(a) and (b)) and TEM images (Figure 4(c) and (d)) show that the resultant NPs had a roughly spherical shape with size average size of 21 nm and 29 nm for ZnO_T and ZnO_T_PLL respectively. In order to obtain the size distribution, DLS analysis was performed. The results reveal the average hydrodynamic diameter of 73.05 nm and 104.82 nm for uncoated (ZnO_T) and coated (ZnO_T_PLL) NPs, respectively (Figure 4(e) and (f)). EDX spectra (Figure 5(a) and (b)) indicate the presence of Zn, O, and C both in ZnO_T and ZnO_T_PLL due to the presence of ZnO and Tween-80. The introduction of N in ZnO_T_PLL attests to the presence of PLL in the NP.

The FTIR analysis shown in **Figures 5(c)** and **(d)**confirms the peak at around 470 cm⁻¹, which corresponds to the stretching vibration of the Zn-O bond present in all the NPs (Khan et al., 2010). The absorption peak at 1450 cm⁻¹ from the spectra of ZnO₋T is due to bending vibration of O-H, which may be accounted for by the interaction of ZnO with the C-H bond of Tween-80 (). A broad peak at 3400 cm⁻¹ in ZnO₋T suggests an abundance of O-H groups present on the surface of ZnO₋T. The addition of a peak at 1590 cm⁻¹ in the ZnO₋T-PLL spectra is due to the introduction of amide groups present in PLL. The broad peak from 3100-3600 cm⁻¹ is due to overlapping of amino and hydroxyl groups, the former introduced from PLL (Babic et al., 2008). The surface charge of ZnO₋T and ZnO₋T-PLL particles were measured by the zeta potential assay. **Supplementary Figure S5** clearly depicts the variation of the surface zeta potential for a wide range of pH. The result shows that the surface charge of ZnO₋T-PLL (4.6 mV) was found to be higher than ZnO₋T (-0.5 mV) at pH 5.5, indicating the greater potential of ZnO₋T-PLL to be attached to the cell surface.

3.3 NP internalization and retention study: In order to evaluate the efficacy of drug uptake and retention of ZnO_T_PLL NPs, they were tested on MCF-7 cells. The MCF-7 cells were chosen to mimic epithelial uptake in cells from the mammary gland, which is the cell type that is generally targeted for breast cancer treatment. Since LSCM coupled with an incubator can be employed for time-lapse 3D imaging, here we implement LSCM based imaging set-up for *in-vitro* testing of particle retention and ROS accumulation in tumor cells. The schematic diagram for the investigation on the particle internalization, cellular retention, and ROS generation is shown in **Figure 1.** In order to depict the interaction between the particles and cells, we performed time-lapse imaging for 5 hours using DIC mode after incubation for two days. This video demonstrates the dynamics of MCF-7 cells and consequent changes in cell morphology with time when treated with ZnO_T_PLL (Supplementary Video S1). However, such a continuous time-lapse generation for three days was avoided as a long-exposure to laser may lead to cell apoptosis.

Although Supplementary video S1 was able to capture the dynamic changes in cells, such imaging cannot be used for quantification of retention of ZnO_T_PLL. In order to image the particle internalization along with the cell height, fluorescent intensity was captured for 38 stacks in order to cover the top-most and bottom-most planes, which varies in a range from 0 to 38µm. Specifically, 3D imaging was performed to obtain the integration of fluorescent signals from individual planes across the layers within a cell. The specific advantages of 3D imaging is shown in Figure 6 through a comparison of 2D and 3D images. It is evident from Figure 6(c) and Supplementary Video S2 that the internalized particles were present at multiple planes. The individual z-scans spanning a depth of 38µm were created by compression of individual 2D images presented in Supplementary Figure S2(i) and (ii).

Similarly, ROS generation at different z-planes are shown in Supplementary Figure S2(b). The result shows how the 3D reconstruction provides accurate signals corresponding to the amount of internalized particles, and ROS generation, when compared to 2D imaging, thereby making the quantification more reliable (Figure 6(a) and (b)). We also present the depth coding for all the cells with internalized particles in Figure 6(d) that clearly indicates that MCF-7 cells are present at different z levels, confirming the necessity of 3D imaging. To further attest to the internalization of the particles inside MCF-7 cells we combined fluorescence imaging and DIC imaging and the merged image in Supplementary Figure S6 shows that the ZnO_T_PLL particles are present inside the cells and not on the surface of the cells.

Since NP retention and drug-mediated cell death is known to be crucial in determining the efficacy of the NP formulation, first, we focus on the investigation of the cellular retention. MCF-7 cells were incubated with 40 µg/mL of ZnO_T_PLL NPs, and the imaging of particle internalization was acquired over 72 hours. Figure 7(a),(b)shows the representative images of particle retention at 0, 12, 24, 36, 48, and 72 hours along with intensity mapping. Since NPs are known to induce apoptosis through the generation of ROS in excess amounts, we focus on investigating the dynamics of the ROS produced in assessing this as the mechanism to induce toxicity in the presence of ZnO_T_PLL NPs. Figure 7(c) and (d) show the time-lapse images corresponding to intracellular ROS generation at various time intervals and corresponding intensity maps in a cell population. Figure 7(e) represents the merged images of cellular internalization and ROS formation.

Specifically, 40 µg/mL concentration ZnO_T_PLL was chosen for this study since the particle internalized was found to be significant at 48 hours for this concentration. The comparison of particle internalization in MCF-7 cells at 0, 12, 24, and 48 hours in the presence of 10 and 40 µg/mL of ZnO_T_PLL NPs and corresponding intensity maps are shown in Supplementary Figure S7. The confocal images of the cells showed a dose-dependent fluorescence intensity with a significantly higher fluorescence signal at 40 µg/mL. The comparative study suggests the suitability of using 40 µg/mL as the concentration to be assessed. Moreover, we performed a study on differential cell toxicity and the preferential killing capability of the ZnO_T_PLL NPs for MCF-7 cells over healthy L929 cells. Supplementary Figure S8 shows that the cell viability of MCF-7 cells was significantly (p<0.0001) lower than normal L929 cells in the presence of ZnO_T_PLL NPs (p<0.0001). The viability of MCF-7 cells was found to be 43.53%, while L929 cells were 83.3% viable post 24 hours of incubation. The results clearly demonstrate the preferential killing of cancerous MCF-7 cells over healthy L929 cells. This study also showed that 40 µg/mL could be used as a subtoxic dose as the normal cells show significantly higher viability (p<0.0001) than cancer cells over a period of 72 hours (Supplementary Figure S8).

Next, we show how LSCM allowed internalization study in single cells through enabling 3D imaging at a higher resolution, which ensured the internalization of the particles in subcellular parts rather than particles being adsorbed on the cell surface. Figure 8 (a) and (b) show the internalization of ZnO_T_PLL in single cells. The result also shows the aggregation of ZnO_T_PLL NP clusters to be localized in the outer cell membrane of the MCF-7 cells up to 12 hours as found in Figure 8(ii) with no significant morphological changes in the cells. Detectable fluorescence at 12 hours post-treatment indicates the starting of ZnO_T_PLL internalization inside the cytoplasm of the MCF-7 cells (Figure 8(a),(b)). It can be concluded that, early phases of ZnO_T_PLL internalization inside the cytoplasm of the cell is not associated with a prominent change in morphology (Figure 8(iii) and Supplementary Figure S9). The presence of higher levels of fluorescence at 48 hours, as evident from images of cellular uptake study, affirms the presence of the ZnO particles in the second day of treatment, which further confirms the cellular retention Figure 8(v). The result shows that LSCM, being a potential tool to evaluate the NP internalization dynamics, can be employed to get an insight into the delivery of ZnO_T_PLL into MCF-7 cells for 72 hours.

Next, we present the simultaneous measurement of ROS in single cells at different times. **Figure 8(c),(d)** shows the intensity of MitoSOX dye and corresponding spatial intensity mapping in single cells. The results show that the ROS formation was rather sporadic up to 12 hours of treatment, owing to the lower amount of NPs present in the cells (**Figure 8(c) and (d)**). A modest increase in ROS formation was observed after 24 hours of treatment. In contrast, at 36 hour, the abundance of red spots indicates a significant increase

in ROS production likely due to accumulation of ZnO_T_PLL NPs in the cytoplasm (**Figure 8(c) and (d)**). The result clearly shows that The NP internalization and ROS accumulation at 72 hours corresponds to complete destruction in cell morphology as a result of cell death(**Figure 8(vi))**. From the above results, it can be concluded that the use of laser scanning helped us to gain a better insight not only in deciphering the internalization dynamics but also to identify the spatial distribution of particles inside single cells. Such spatial distribution study in single cells indicates a strong interdependence between ZnO_T_PLL particle retention and ROS generation in NPs.

- 3.4 Time course of cell viability for 72 hours: In order to assess the correlation between NP internalization, ROS formation, and cell death in a heterogeneous cell population, a live-dead imaging assay was conducted at 40 μ g/mL concentration at the same time points, i.e., 0, 12, 24, 36 and 72 hours (**Figure 9**). As evident from **Figure 9**, early time points up to 12 h (cell viability of 78.41%) show fewer cells with PI uptake, attributed to the lower uptake of NPs. The results show that following 36 h, the percentage of cells with PI uptake increases and gets associated with the disruption of membrane integrity (viability=16.78%). Hence, it can be concluded that significant toxicity (cell viability= 5.02%) towards tumor cells can be induced at 48 h through the application of 40μ g/mL ZnO-T-PLL particles (**Figure 9**). Such ROS-mediated cell death can be attributed due to the capability of ZnO NPs in inducing ROS like hydroxyl and superoxide radicals attributed to their semiconductor properties and to perturb electronic transfer processes in the cell (Ancona et al., 2018)).
- 3.5 Quantification of NP internalization, ROS generation, and cell viability: Since the imaging results indicated the interdependence between ZnO_T_PLL particle retention and ROS generation, we further performed quantification of NP retention, ROS generation, and cell viability dynamics. The time course of particle retention and percentage increase in ROS has been depicted in Figure 10 (a) and (b). The percentage cell viability of MCF-7 cells with respect to time has been depicted in Figure 10(c). The quantification of cellular internalization, ROS accumulation, and cell viability was performed based on numerous images taken simultaneously at a single time point. The result suggests a sigmoidal response for internalization of ZnO_T_PLL NPs with time. The results also indicate that it is possible to develop an in vitro assay for assessing the efficacy of the nanoformulation as an anticancer agent through the proposed imaging set up.

Additionally, we performed the fitting of various functions and found that a pseudo-first-order kinetic model can be fitted to the internalization of particles with time (**Figure 10(a)**). A positive Pearson's correlation value between percentage particle internalization and ROS generated (r=0.942) shows that there is a strong correlation between ROS generation and particle internalization. On the other hand, negative Pearson's correlation values between percentage particle internalization and cell viability (r=-0.9838) and ROS generation and cell viability (r=-0.98175) indicate the synergy between long term particle retention and toxicity towards tumor cells. The time-dependent analysis of intracellular events indicates a possible mechanism of apoptosis through mitochondrial ROS generation in cells when invaded by ZnO_T_PLL NPs. A schematic of these intracellular events has been shown in **Figure 10(d)**. Overall, it can be concluded that the confocal microscopy assisted investigation of mitochondrial ROS production inside the MCF-7 cells can also be used for deciphering mechanisms underlying the intracellular events.

4. Discussion

Fluorescent nanoformulations have been an attractive research topic in the field of cancer research both for imaging and therapeutic purposes. Specifically, ZnO NPs are one of the potential anticancer agents against MCF-7 cells and can be used for treatment of breast cancer (Sadhukhan et al., 2019; Hong et al., 2011; Ma et al., 2015; Sureshkumar et al., 2017; Gupta et al., 2015; Kavithaa et al., 2016; Salari et al., 2020; Boroumand Moghaddam et al., 2017; Farasat et al., 2020; Lestari et al., 2018; Wahab et al., 2014). However, quantitative imaging of spatial distribution of NPs in living cells over days was not investigated much. A detailed study on cell-NP interaction using time-lapse microscopy assumes importance in assessing the toxicity as well as therapeutic potential. In this paper, we performed optimization of the NP synthesis to achieve the fluorescence that can be used for 3D imaging for three days in cell culture medium. In order

to achieve this, Tween-80 assisted fluorescent ZnO NPs were coated with PLL. The fluorescence in this case might be attributed to the chemically bonded oxygen molecules of the Tween-80. These act as scavengers of the photogenerated electrons and transfer them to deep traps. These electrons upon recombination with trapped holes may result in a recombination centre for visible emission (Khan et al., 2010). When characterized, there was a disparity in the aerodynamic and hydrodynamic diameter of the particles, which could be accounted to the fact that ZnO being an amphoteric oxide, undergoes hydrolysis in water. This results in the formation of a hydroxide coating, ultimately leading to physical adsorption of water molecules on the surface (Wang et al., 2017).

As evident from the increased hydrodynamic diameter in ZnO_T_PLL NPs, it can be concluded that PLL coating increased the hydrophilic nature of the NPs. Hanley et al. demonstrated the preferential uptake of ZnO NPs in cancerous cells compared to healthy T cells (Hanley et al., 2008). It has also been hypothesized that the hydrophilicity of the synthesized particles may remain beneficial for passive targeting owing to its ability to escape macrophage capture (Allahverdiyev et al., 2018). Although future experiments need to be conducted, it can be expected that ZnO_T_PLL NPs being hydrophilic may overcome the threat of macrophage capture generally found in lipid and polymeric particles.

There is limited information on hydrolysis of zinc-oxide inside lysosomes due to the acidic pH of cancer cells during long-term imaging (; Xia et al., 2008). Although further imaging experiments need to be performed to investigate on this matter using lysosomal staining (Dong et al., 2018; Xia et al., 2008), in this work, we performed the measurement of zeta potential to check the stability of the synthesized zinc oxide material over a range of pH . Our results showed that the PLL coating leads to an improved range of zeta potential which provides a roadmap to synthesize a reasonably stable particle. At the same time the zeta potential remains in the favorable range for the attachment of the ZnO particles on the surface of MCF-7 cells. Poly-L-lysine being a cationic polymer, it exerts a layer of positive surface charge. However, the stability of the particle can be further improved by coating the fluorescent ZnO with a thicker PLL layer by altering the PLL concentration while coating the particles. This may lead to a tailored particle that is stable as well as suitable for faster attachment to the cell surface.

Our current study focuses on imaging of MCF-7 cells at 40 μ g/mL of ZnO_T_PLL upto 72 hours. However, a future work is rather needed for a detailed study on retention dynamics at various concentrations of ZnO NPs. Since it has been found that the fluorescent ZnO nanostructures in the range 100-400 nm induce preferential killing in MCF-7 cells compared to L929 cells at 40 μ g/mL, we chose to perform the 3D imaging study at this concentration. Additionally, a co-culture study was performed to show that normal T cells can be maintained at 85% viability in the range of 10-40 μ g/mL concentration of FITC-tagged fluorescent ZnO particles, whereas cancerous T cells were found to be less than 10% viable at 40 μ g/mL NP concentration (Hanley et al., 2008).

Also, there are multiple studies on non-fluorescent ZnO particles for which the viability of normal cells (HBL100 and MCF10A) were found to be significantly higher than MCF-7 cells in presence of ZnO nanostructure (Kavithaa et al., 2016; Farasat et al., 2020). It has been shown that 60% viability of HBL100 cells can be retained within 48 hour using ZnO nanorod of size range from 70 nm to 140 nm at a concentration of 10-20 $\mu g/mL$ (Kavithaa et al., 2016). Based on the concentration range and particle size of the existing ZnO NP experiments (Table S1), here we choose 40 $\mu g/mL$ to track the NP distribution and ROS generation while maintaining lower cytotoxicity to normal cells. Although, a comparison of cell viability between MCF-7 and L929 in presence of the synthesized NPs shows a preferential killing of the MCF-7 breast cancer cell line (Supplementary Figure S8), further optimization can be done for minimization of toxicity towards healthy cells.

Although generation of ROS is taken as a mechanism for inducing toxicity in cancer cells, there is limited data on spatiotemporal ROS dynamics induced by ZnO particles in MCF-7 cells (Gupta et al., 2015). Previously, Gupta et al. (Gupta et al., 2015) has shown the evidence of ROS generation with varying FITC tagged ZnO NP concentration at 24 hr, but the correlation between time course of particle internalization and ROS formation was not evident.

One of the limitations of the current study is that it focuses on monitoring of cell viability in individual cultures of MCF-7 and L929 cells. However, a comparison cell-NP interaction in a co-cultured MCF-7 and L929 cells will be required for gaining insight on the preferential internalization of these particles in the MCF-7 cells. Similarly, the formation of ROS generated as a result of oxidative phosphorylation can be monitored in normal cells as well as tumor cells inside the co-culture model. In order to understand the molecular interaction, a mechanistic model can be obtained for simultaneous prediction of internalization, ROS and viability.

Previously, it has been shown that fluorescent ZnO acts as a promising therapeutic agent for reducing the tumor volume from 1.2cc to 0.6cc in 15 days (breast tumor) in rat models (Hong et al., 2015). Very recently, non-fluorescent ZnO has been tested previously on rat models and has been seen to successfully reduce breast cancer tumor volume (Tanino et al., 2020; . Since the proposed work forms a solid basis for choosing ZnO particles as a potential candidate for treating breast cancer through *in vitro* imaging assay, we propose that the PLL coated ZnO NPs can further be tested *in vivo* in a rat model. Some of the recent investigations have revealed that ZnO can be effective as anti-proliferative agent and inhibition agent against various viral strains such as H1N1 and simplex viruses (Ghaffari et al., 2019; Tavakoli et al., 2018; Abdul et al., 2020; Faten & Ibrahim, 2018). Hence, future studies can also be conducted on the effectiveness of ZnO_T_PLL as an antiviral agent.

5. Conclusion

To the best of our knowledge, this is the first instance of synthesis of poly-L-lysine coated fluorescent ZnO NPs (ZnO_T_PLL) that can be used for time-lapse microscopy upto 72 hours in DMEM media using LSCM without photobleaching. Specifically, we show that 3D live imaging can be implemented to quantify the cellular retention of ZnO particles in preclinical evaluations based on *in vitro* assays. Moreover, we demonstrate the (i) cellular uptake of the fluorescent ZnO NPs leads to increased ROS formation (ii) reduction of MCF-7 cell viability at a concentration of $40\mu g/mL$ and (iii) simultaneous monitoring of dynamic pattern in ZnO distribution in MCF-7 cells and ROS generation. The proposed particle can be further improved in terms of targeting capability through specific functionalization of the NPs. Furthermore, the proposed volumetric imaging techniques can be used for optimization of the NP dosage. On the basis of current research, the fluorescent particles can be further tested in animals to check whether it is possible to eliminate them through the immune system.

Acknowledgements

The authors acknowledge the research facilities provided by Indian Institute of Technology Kharagpur, India and Indian Institute of Technology Hyderabad, India. The authors also acknowledge Mr. K. Venkateswarlu from Indian Institute of Technology Hyderabad, India for his guidance in writing the paper and Mr. Nilanjan Dutta from Indian Institute of Technology Madras, India for his valuable contribution in statistical data analysis.

Conflict of Interests: The authors declare that there are no conflict of interests.

Authorship

Aishee Dey, Lopamudra Giri and Sudarsan Neogi designed research; Aishee Dey, Suman Gare, Sarpras Swain, Proma Bhattacharya and Vaibhav Dhyani performed research and data collection; Aishee Dey, Suman Gare, and Lopamudra Giri performed data analysis; and Aishee Dey, Sudarsan Neogi and Lopamudra Giri wrote the paper.

References

Abdul, W., Muhammad, A., Ullah, K. A., Asmat, A., & Abdul, B. (2020). Role of nanotechnology in diagnosing and treating COVID-19 during the Pandemi. *International Journal of Clinical Virology*. doi:10.29328/journal.ijcv.1001017

- Allahverdiyev, A. M., Parlar, E., Dinparvar, S., Bagirova, M., & Abamor, E. Ş. (2018). Current aspects in treatment of breast cancer based of nanodrug delivery systems and future prospects. *Artificial Cells, Nanomedicine, and Biotechnology*, 46(sup3), S755–S762.
- Ancona, A., Dumontel, B., Garino, N., Demarco, B., Chatzitheodoridou, D., Fazzini, W., ... Cauda, V. (2018). Lipid-Coated Zinc Oxide Nanoparticles as Innovative ROS-Generators for Photodynamic Therapy in Cancer Cells. *Nanomaterials (Basel, Switzerland)*, 8(3). doi:10.3390/nano8030143
- Babic, M., Horák, D., Trchová, M., Jendelová, P., Glogarová, K., Lesný, P., ... Syková, E. (2008). Poly(L-lysine)-modified iron oxide nanoparticles for stem cell labeling. *Bioconjugate Chemistry*, 19(3), 740–750.
- Boroumand Moghaddam, A., Moniri, M., Azizi, S., Abdul Rahim, R., Bin Ariff, A., Navaderi, M., & Mohamad, R. (2017). Eco-Friendly Formulated Zinc Oxide Nanoparticles: Induction of Cell Cycle Arrest and Apoptosis in the MCF-7 Cancer Cell Line. *Genes*, 8(10). doi:10.3390/genes8100281
- Chen, X., Chen, C.-B., Udalagama, C. N. B., Ren, M., Fong, K. E., Yung, L. Y. L., ... Watt, F. (2013). High-Resolution 3D Imaging and Quantification of Gold Nanoparticles in a Whole Cell Using Scanning Transmission Ion Microscopy. *Biophysical Journal*. doi:10.1016/j.bpj.2013.02.015
- Choudhury, S. R., Mandal, A., Chakravorty, D., Gopal, M., & Goswami, A. (2013). Evaluation of physicochemical properties, and antimicrobial efficacy of monoclinic sulfur-nanocolloid. *Journal of Nanoparticle Research*. doi:10.1007/s11051-013-1491-y
- Dias, A., Werner, M., Ward, K. R., Fleury, J.-B., & Baulin, V. A. (2019). High-throughput 3D visualization of nanoparticles attached to the surface of red blood cells. *Nanoscale*. doi:10.1039/c8nr09960j
- Dong, K., Wang, Z., Zhang, Y., Ren, J., & Qu, X. (2018). Metal-Organic Framework-Based Nanoplatform for Intracellular Environment-Responsive Endo/Lysosomal Escape and Enhanced Cancer Therapy. *ACS Applied Materials & Interfaces*, 10(38), 31998–32005.
- Farasat, M., Niazvand, F., & Khorsandi, L. (2020). Zinc oxide nanoparticles induce necroptosis and inhibit autophagy in MCF-7 human breast cancer cells. *Biologia*. doi:10.2478/s11756-019-00325-9
- Faten, F., & Ibrahim, S. R. (2018). Comparing Surface Chemical Modifications of Zinc Oxide Nanoparticles for Modulating their Antiviral Activity against Herpes Simplex Virus Type-1. *International Journal of Nanoparticles and Nanotechnology*. doi:10.35840/2631-5084/5521
- Ghaffari, H., Tavakoli, A., Moradi, A., Tabarraei, A., Bokharaei-Salim, F., Zahmatkeshan, M., ... Ataei-Pirkooh, A. (2019). Inhibition of H1N1 influenza virus infection by zinc oxide nanoparticles: another emerging application of nanomedicine. *Journal of Biomedical Science*, 26(1), 70.
- Gimenez, Y., Busser, B., Trichard, F., Kulesza, A., Laurent, J. M., Zaun, V., ... Motto-Ros, V. (2016). 3D Imaging of Nanoparticle Distribution in Biological Tissue by Laser-Induced Breakdown Spectroscopy. *Scientific Reports*, 6, 29936.
- Gupta, J., Bhargava, P., & Bahadur, D. (2015). Fluorescent ZnO for imaging and induction of DNA fragmentation and ROS-mediated apoptosis in cancer cells. *Journal of Materials Chemistry. B, Materials for Biology and Medicine*, 3(9), 1968–1978.
- Hanley, C., Layne, J., Punnoose, A., Reddy, K. M., Coombs, I., Coombs, A., ... Wingett, D. (2008). Preferential killing of cancer cells and activated human T cells using ZnO nanoparticles. *Nanotechnology*. doi:10.1088/0957-4484/19/29/295103
- Hong, H., Shi, J., Yang, Y., Zhang, Y., Engle, J. W., Nickles, R. J., ... Cai, W. (2011). Cancer-targeted optical imaging with fluorescent zinc oxide nanowires. *Nano Letters*, 11(9), 3744–3750.
- Hong, H., Wang, F., Zhang, Y., Graves, S. A., Eddine, S. B. Z., Yang, Y., ... Cai, W. (2015). Red fluorescent zinc oxide nanoparticle: a novel platform for cancer targeting. *ACS Applied Materials & Interfaces*, 7(5), 3373–3381.

- Hussein, A., & Ministry of health –clinical pathology center. (2017). Comparative Evaluation Of Anticancer Potential Of Moringaoleifera, Ganodermalucidumand Silver Nanoparticles Against Breast And Liver Cancer Cell Lines And Related Pro And Anti Apoptotic Genes Profile. *International Journal of Scientific Research and Management*. doi:10.18535/ijsrm/v5i3.12
- Jiang, J., Pi, J., & Cai, J. (2018). The Advancing of Zinc Oxide Nanoparticles for Biomedical Applications. *Bioinorganic Chemistry and Applications*, 2018, 1062562.
- Kavithaa, K., Paulpandi, M., Ponraj, T., Murugan, K., & Sumathi, S. (2016). Induction of intrinsic apoptotic pathway in human breast cancer (MCF-7) cells through facile biosynthesized zinc oxide nanorods. *Karbala International Journal of Modern Science*. doi:10.1016/j.kijoms.2016.01.002
- Khader, A., & Arinzeh, T. L. (2020). Biodegradable zinc oxide composite scaffolds promote osteochondral differentiation of mesenchymal stem cells. *Biotechnology and Bioengineering*, 117(1), 194–209.
- Khan, Y., Durrani, S. K., Mehmood, M., Ahmad, J., Riaz Khan, M., & Firdous, S. (2010). Low temperature synthesis of fluorescent ZnO nanoparticles. *Applied Surface Science*. doi:10.1016/j.apsusc.2010.09.011
- Kiefer, R., Jurisic, M., Dahlem, C., Koch, M., Schmitt, M. J., Kiemer, A. K., ... Breinig, F. (2020). Targeted delivery of functionalized PLGA nanoparticles to macrophages by complexation with the yeast Saccharomyces cerevisiae. *Biotechnology and Bioengineering*. doi:10.1002/bit.27226
- Lestari, U., Mufti, N., Lutfiyah, D. A., Fitriyah, U., & Annisa, Y. (2018). UV Irradiation Enhanced In-Vitro Cytotoxic Effects of ZnO Nanoparticle on Human Breast Cancer. *Journal of Physics: Conference Series*. doi:10.1088/1742-6596/1093/1/012046
- Marsich, L., Bonifacio, A., Mandal, S., Krol, S., Beleites, C., & Sergo, V. (2012). Poly-L-lysine-coated silver nanoparticles as positively charged substrates for surface-enhanced Raman scattering. *Langmuir: The ACS Journal of Surfaces and Colloids*, 28(37), 13166–13171.
- Ma, Y.-Y., Ding, H., & Xiong, H.-M. (2015). Folic acid functionalized ZnO quantum dots for targeted cancer cell imaging. *Nanotechnology*, 26(30), 305702.
- Ramos-Gomes, F., Ferreira, N., Kraupner, A., Alves, F., & Andrea Markus, M. (2020). Ex vivo Live Cell Imaging of Nanoparticle-Cell Interactions in the Mouse Lung. *Frontiers in Bioengineering and Biotechnology*. doi:10.3389/fbioe.2020.588922
- Sadhukhan, P., Kundu, M., Chatterjee, S., Ghosh, N., Manna, P., Das, J., & Sil, P. C. (2019). Targeted delivery of quercetin via pH-responsive zinc oxide nanoparticles for breast cancer therapy. *Materials Science & Engineering. C, Materials for Biological Applications*, 100, 129–140.
- Salari, S., Neamati, A., Tabrizi, M. H., & Seyedi, S. M. R. (2020). Green-synthesized Zinc oxide nanoparticle, an efficient safe anticancer compound for human breast MCF7 cancer cells. *Applied Organometallic Chemistry*. doi:10.1002/aoc.5417
- Semkina, A. S., Abakumov, M. A., Skorikov, A. S., Abakumova, T. O., Melnikov, P. A., Grinenko, N. F., ... Chekhonin, V. P. (2018). Multimodal doxorubicin loaded magnetic nanoparticles for VEGF targeted theranostics of breast cancer. *Nanomedicine: Nanotechnology, Biology, and Medicine*, 14(5), 1733–1742.
- Sivakumar, P., Lee, M., Kim, Y.-S., & Shim, M. S. (2018). Photo-triggered antibacterial and anticancer activities of zinc oxide nanoparticles. *Journal of Materials Chemistry*. B, Materials for Biology and Medicine, 6 (30), 4852–4871.
- Song, C., Zhong, Y., Jiang, X., Peng, F., Lu, Y., Ji, X., ... He, Y. (2015). Peptide-Conjugated Fluorescent Silicon Nanoparticles Enabling Simultaneous Tracking and Specific Destruction of Cancer Cells. *Analytical Chemistry*, 87(13), 6718–6723.
- Sureshkumar, S., Jothimani, B., Sridhar, T. M., Santhosh, A., & Venkatachalapathy, B. (2017). Synthesis of Hexagonal ZnO-PQ7 Nano Disks Conjugated with Folic Acid to Image MCF 7 Cancer Cells. *Journal*

of Fluorescence. doi:10.1007/s10895-016-1932-y

Tang, F., Wang, C., Wang, X., & Li, L. (2015). Facile Synthesis of Biocompatible Fluorescent Nanoparticles for Cellular Imaging and Targeted Detection of Cancer Cells. *ACS Applied Materials & Interfaces*, 7(45), 25077–25083.

Tanino, R., Amano, Y., Tong, X., Sun, R., Tsubata, Y., Harada, M., ... Isobe, T. (2020). Anticancer Activity of ZnO Nanoparticles against Human Small-Cell Lung Cancer in an Orthotopic Mouse Model. *Molecular Cancer Therapeutics*. doi:10.1158/1535-7163.mct-19-0018

Tavakoli, A., Ataei-Pirkooh, A., Mm Sadeghi, G., Bokharaei-Salim, F., Sahrapour, P., Kiani, S. J., ... Monavari, S. H. (2018). Polyethylene glycol-coated zinc oxide nanoparticle: an efficient nanoweapon to fight against herpes simplex virus type 1. *Nanomedicine*, 13(21), 2675–2690.

Venkateswarlu, K., Suman, G., Dhyani, V., Swain, S., Giri, L., & Samavedi, S. (2020). Three-dimensional imaging and quantification of real-time cytosolic calcium oscillations in microglial cells cultured on electrospun matrices using laser scanning confocal microscopy. *Biotechnology and Bioengineering*. doi:10.1002/bit.27465

Wahab, R., Siddiqui, M. A., Saquib, Q., Dwivedi, S., Ahmad, J., Musarrat, J., ... Shin, H.-S. (2014). ZnO nanoparticles induced oxidative stress and apoptosis in HepG2 and MCF-7 cancer cells and their antibacterial activity. *Colloids and Surfaces B: Biointerfaces*. doi:10.1016/j.colsurfb.2014.02.038

Wang, J., Lee, J. S., Kim, D., & Zhu, L. (2017). Exploration of Zinc Oxide Nanoparticles as a Multitarget and Multifunctional Anticancer Nanomedicine. ACS Applied Materials & Interfaces, 9(46), 39971–39984.

Wu, D., Si, M., Xue, H.-Y., & Wong, H.-L. (2017). Nanomedicine applications in the treatment of breast cancer: current state of the art. *International Journal of Nanomedicine*, 12, 5879–5892.

Xia, T., Kovochich, M., Liong, M., Madler, L., Gilbert, B., Shi, H., ... Nel, A. E. (2008). Comparison of the mechanism of toxicity of zinc oxide and cerium oxide nanoparticles based on dissolution and oxidative stress properties. *ACS Nano*, 2(10), 2121–2134.

Zhang, Y., Nayak, T., Hong, H., & Cai, W. (2013). Biomedical Applications of Zinc Oxide Nanomaterials. Current Molecular Medicine. doi:10.2174/1566524013666131111130058

Figure Legends

Figure 1: The schematic for the workflow for the synthesis of ZnO_T_PLL nanoparticles and measurement of retention dynamics and ROS accumulation using 3D imaging by LSCM.

Figure 2: Fluorescence level in ZnO_T nanoparticles as a function of percentage of Tween-80 (v/v). (a) 3D imaging of particles corresponding to 8%, 12%, 14%, and 20% Tween-80. (b) Bar plot representation of fluorescent intensities for particles when 8%, 10%, 12%, 14%, and 20% Tween-80 was used. Scale bar in all panels represents 200 μ m. p<0.0001.

Figure 3: Comparison of ZnO_T and ZnO_T_PLL fluorescence level in DMEM medium for three days. 3D reconstruction of fluorescent images for (a) ZnO_T and (b) ZnO_T_PLL at 0, 12, 24, 48 and 72 hours. (c) The box plot representation of the fluorescence intensities of ZnO_T and ZnO_T_PLL at various time points, including 0, 12, 24, 48, and 72 h. A statistical test was performed (* indicates p<0.0001). Scale bar in all panels represents 200 μ m.

Figure 4: Morphology of ZnO_T and ZnO_T_PLL nanoparticles. SEM images of (a) ZnO_T_PLL and (b) ZnO_T, TEM images of (c) ZnO_T_PLL and (d) ZnO_T confirm the nanoarchitecture of the prepared samples. Hydrodynamic size distribution analysis of (e) ZnO_T_PLL and (f) ZnO_T has been depicted by DLS. Scale bar in all panels represents 50 nm.

Figure 5: Elemental analysis of (a) ZnO₋T and (b) ZnO₋T_PLL nanoparticles by using EDX. FTIR analysis of (c) ZnO₋T and (d) ZnO₋T_PLL nanoparticles show the various functional groups present.

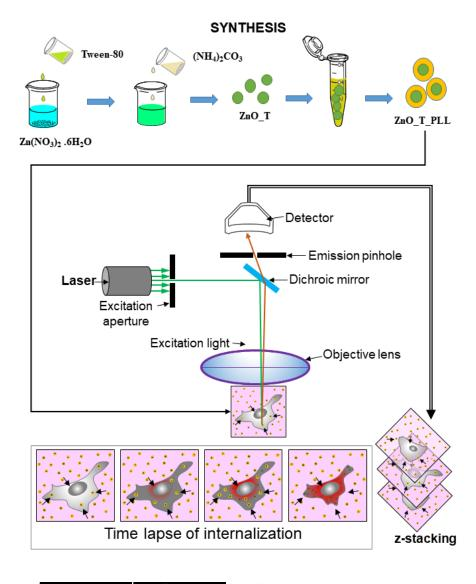
Figure 6: Comparison between individual z-stack (2D) and compressed 2D images from multiple stacks (3D). (a) Compressed 2D images for MCF-7 cells obtained from multiple stacks, (A) DIC images, (B) internalized ZnO_T_PLL, and (C) reactive oxygen species after 36 hours of incubation with nanoparticles. (b) Individual z-stack images for MCF-7 cells, (A) DIC image, (B) internalized ZnO_T_PLL, and (C) reactive oxygen species after 36 hours of incubation with nanoparticles. (c) 3D reconstruction of (A) internalized ZnO_T_PLL, (B) ROS in MCF-7 cells. (d) ZnO_T_PLL internalization and subsequent depth coding to demonstrate the presence of cells at different z levels. Scale bar in all panels represents 100 μm.

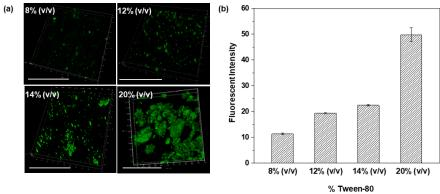
Figure 7: Simultaneous mapping of cellular retention of ZnO_T_PLL and ROS generation in MCF-7 cell population using LSCM. Incubation of cells with ZnO_T_PLL was performed in the incubator attached with the microscope. Time-lapse images for ZnO_T_PLL Internalization and ROS generation are presented in the form of compressed z-stacks. (a) Cellular retention of ZnO_T_PLL nanoparticles during incubation MCF-7 cells with 40µg/mL of nanoparticles, (b) Spatial fluorescent intensity mapping of the internalized particles at 0,12, 24, 36, 48, and 72 hours. (c) Time-lapse images of mitochondrial ROS (stained with MitoSOX Red) at 0,12, 24, 36, 48, and 72 hours. (d) Spatial fluorescent intensity mapping of ROS generation. (e) Merged window representing both internalized Zno_T_PLL and ROS generation. Scale bar in all panels represents 100 μm.

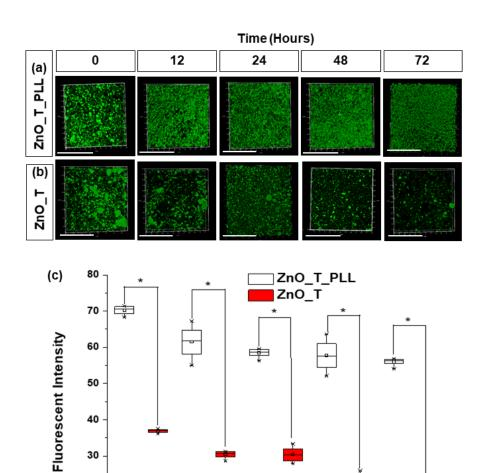
Figure 8: ZnO_T_PLL induced ROS production in single cells during incubation with $40\mu g/mL$ of nanoparticles. Time course of (a) ZnO_T_PLL internalization, (b) Spatial intensity map of internalization, (c) mitochondrial ROS generation and (d) Spatial intensity map of ROS generation at 0, 12, 24, 36, 48 and 72hours. Imaging was performed by laser scanning confocal microscopy after staining with MitoSOX Red. Spatial intensity map was generated from compressed 3D images of ROS accumulation by Image-J software to demonstrate the varying concentration of mitochondrial ROS production. The relative concentrations are depicted by the color intensity with a legend indicated at the right side of the figure. Scale bar in all panels represents 20 μ m.

Figure 9: Effect of ZnO_T_PLL nanoparticles on MCF-7 cell viability. (a)-(e) Time-lapse images MCF-7 cells incubated with $40\mu g/mL$ of nanoparticles at 0, 12, 24, 36, 48 and 72 hours. Live-dead cell assay was performed by staining with calcein (green) and propidium iodide (red), respectively, where green and red denote live cells and nucleus of dead cells obtained. Scale bar in all panels represents 750 μm .

Figure 10: Correlation between the temporal dynamics of nanoparticle internalization, ROS accumulation, and cell viability. Time course of (a) ZnO_T_PLL internalization in MCF-7 cell, (b) Percentage ROS generation, (c) cell viability of MCF-7 cell, (d) Schematic of a hypothetical pathway for ROS generation facilitated by ZnO_T_PLL and consequent cell death in MCF-7 population.





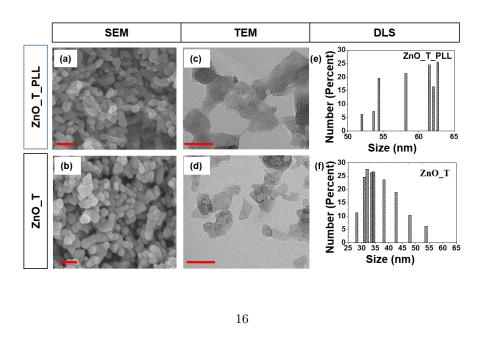


30

20

10

0 h



12 h

24 h

Time (Hours)

48 h

72 h

